Some Practical Aspects of Slant Wave Stacks

by Philip S. Schultz

In our previous discussions of slant wave stacked data, we had implicitly assumed that a stack over any desired ray parameter, $p = \frac{\sin\theta}{v}$, could be done, with the resultant data display precisely that which we would have obtained from a downgoing cylindrical wave propagating at some angle, θ, to the vertical. This for the most part remains true, but only with respect to two important practical considerations: our data (in the form of common shot or common geophone gathers) are 1) of finite spatial and temporal extent, and 2) discretely sampled in space and time. The first item imposes on us the problem of end effects, while the second can introduce aliasing.

The manner in which the truncation of the data can produce end effects is shown in Figure 1. The only contribution to a slant sum should be from the region of tangency, but a small contribution will arise from the termination of the data at the near and far offsets. These end effects have been noticed by us in our previous attempts to slant stack field data. The far trace end effect (the dotted line in Figure 1) can be easily seen in the slant stacks in our previous report (see Schultz, p. 102 ff., SEP-7). They appear as a "ghosting" of the sea floor at $t \gtrsim 2$ seconds. The near trace end effect (the dashed line in Figure 1) cannot as readily be identified in these stacks, but must certainly be present at closer proximity to the primary energy. We suspect that it was this near trace end effect which contaminated the primary waveform and made Noah's deconvolution impossible.

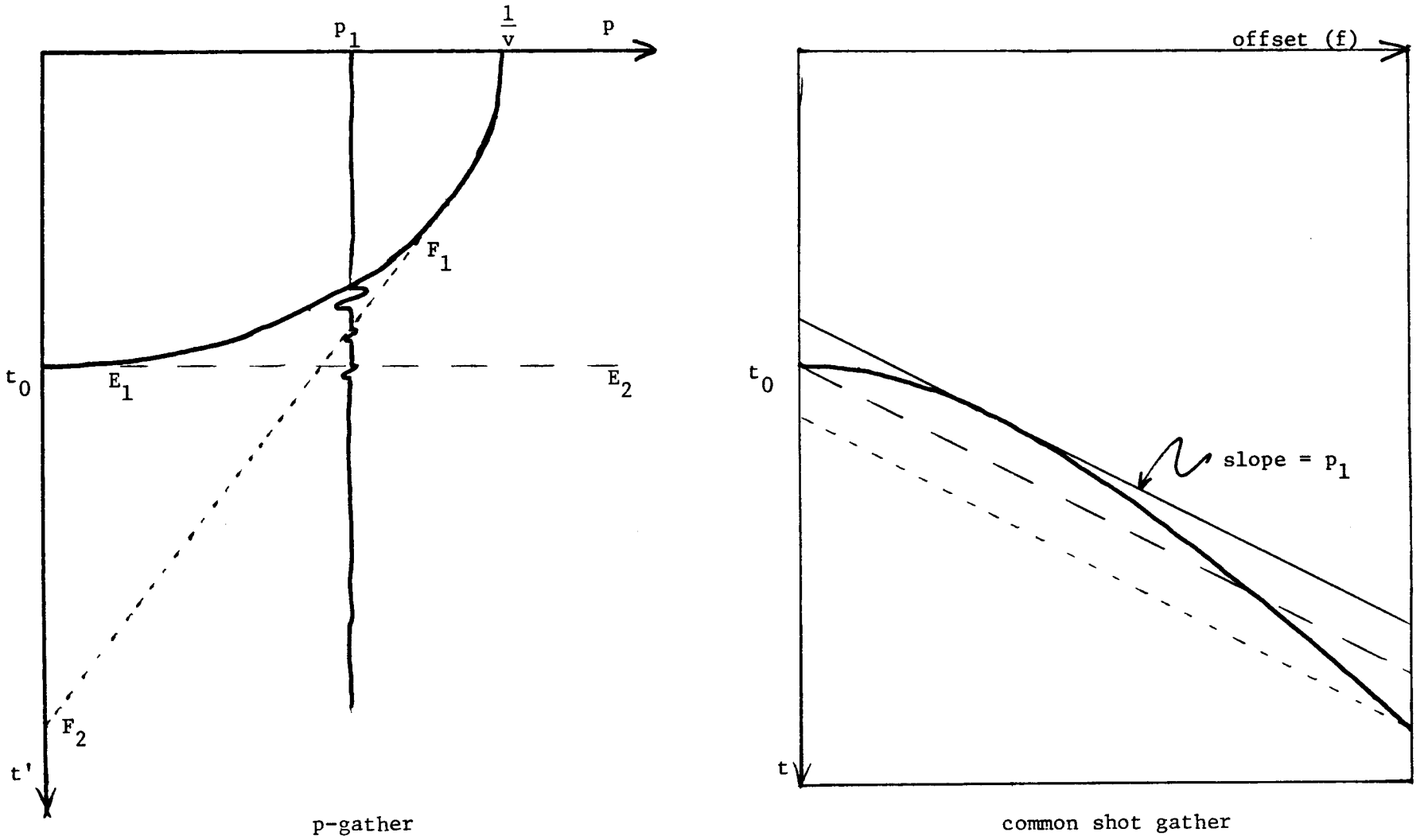

Figure 1. The end effect problem. The frame to the right shows a common shot (or geophone) gather with a single hyperbolic event portrayed. If we do a slant stack over ray parameter $p = p_1$, we get the main

(cont'd. on following page)

Fig. 1 (Cont'd.).

contribution in the stationary phase summation at the point of tangency, shown as the solid sloping line. The two other sloping lines, the dashed and the dotted lines, show non-zero contributions to the summation due to the near line E_1E_2 and far line F_1F_2 offset truncations of the data.

The frame to the left shows the p-gather produced from the common shot gather. The portion of an ellipse drawn as a solid line is the main event. Its intercepts are at $t = t_0$ and $p = 1/v$. The dashed and dotted lines show where the two end effects map into this domain. The trace at $p = p_1$ is drawn.

There must certainly be many approaches that will be effective in reducing end effects, but the one that we are now using was suggested by Bjorn Engquist, and has the advantage of being computationally cheap.

Figure 2 shows how we can sample past the end traces if we have some knowledge of rms velocity. Sampling n traces off the end of the cable can be equivalenced to resampling and summing a region δt, of the last trace. But rather than sampling the last trace so coarsely (shown by the small circles in Figure 2), we can instead use all time points in the region δt to insure against possible aliasing.

Observing Figure 2, we can write immediately

$$\left[\left(\frac{dt}{df}\right)_e - \left(\frac{dt}{df}\right)_s \right] n \Delta f = \delta t \qquad (1)$$

where f is the offset coordinate, subscript "e" refers to the trajectory of the event, subscript "s" refers to the trajectory of the slant stack summation, Δf is the horizontal sampling interval (group spacing), and n is the number of traces off the end of the cable.

Let

$$\delta t = \gamma \Delta t \qquad (2)$$

where Δt is the sampling interval on the time axis, and γ is some number (not necessarily integral).

From the equation for the event, e,

$$t^2 = t_0^2 + \frac{f^2}{v_{rms}^2} \qquad (3)$$

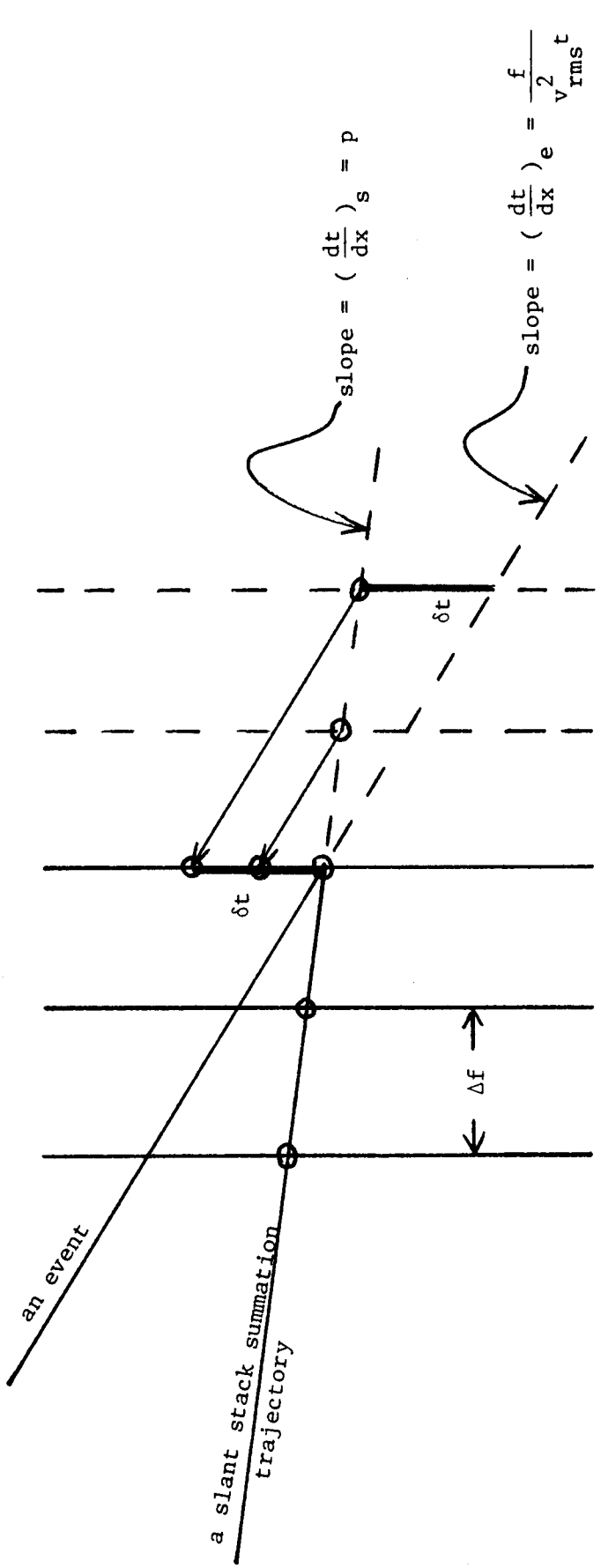

Figure 2. An approach to reducing end effects. The final three traces of a 48-trace common shot (or geophone) gather is shown with two hypothetical traces added. The small circles show where the traces are to be sampled in the summation. With knowledge of velocity, sampling of traces off the end of the cable can be approximated by sampling the last trace in the manner suggested in the figure. Formulas are derived in the text. This trick can also be applied to the inner trace.

we have

$$\left(\frac{dt}{df}\right)_e = \frac{f}{t\, v_{rms}^2} \tag{4}$$

and trivially,

$$\left(\frac{dt}{df}\right)_s = p \tag{5}$$

giving an expression for γ ,

$$\gamma = n\left(\frac{\Delta f}{\Delta t}\right)\left(\frac{f}{t\, v_{rms}^2} - p\right) \tag{6}$$

The above result tells us how many time points to sum "upward" on the last trace ($f = f_{max}$) or "downward" on the first trace ($f = f_{min}$) to include n traces off the end of the cable into the sum.

Our choice of n must be made moderate because of our uncertainty in v_{rms} , and because the slope of the event will change between f_{max} and f_{max+n} . We are currently using $n = 6$.

The form of equation (6) shows that for a stack over a single value of p , the first and last traces in the common shot (geophone) gather can be recomposed by replacing each time point by a sum over the proper interval $\gamma\, \Delta t$, predicted by equation (6). The slant stack can then procede simply.

Figure 3 shows how aliasing can be introduced into the slant stack. When the slant sum trajectory intercepts an event at a large angle, finite spatial sampling will at some point lead to aliasing.

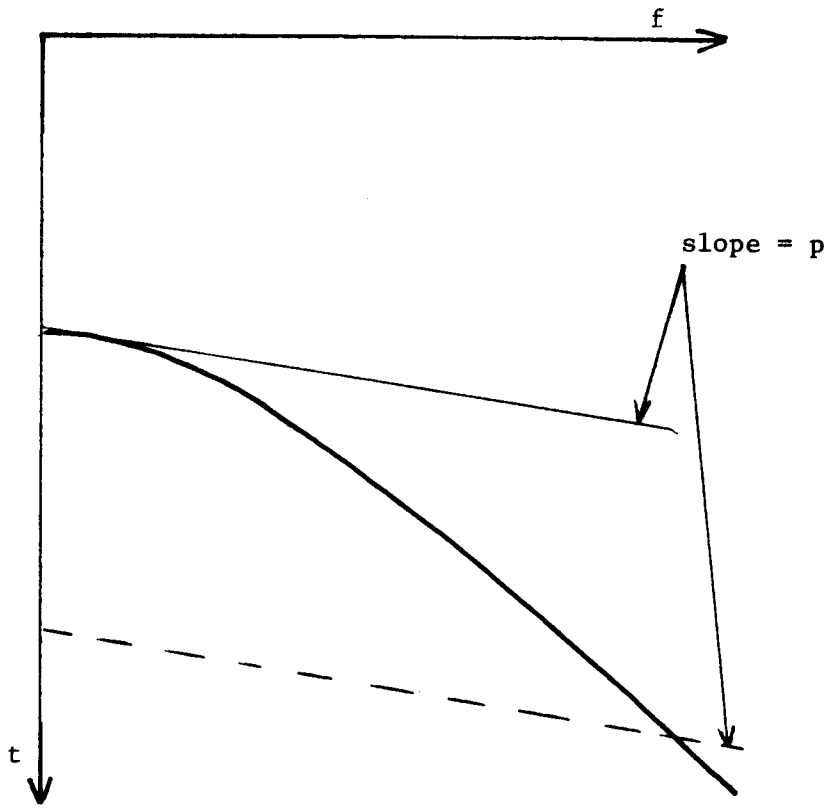

Figure 3. A common geophone gather showing slant summation trajectory for some p. The solid sloping line shows the trajectory for the summation at point of tangency. The dashed line shows another summation trajectory which should add to zero (or whatever small quantity is predicted by the continuous solution). However, since at this point we are summing across the event at a steep angle, the finite sampling interval in the x coordinate can cause aliasing, thereby introducing spurious energy into the slant stack.

As with end effects, there are many workable methods to eliminate or reduce this type of aliasing. Our approach is to "window" the data so that we include only those data which we expect will contribute to the slant sum.

Figure 4 shows that the general shape of the anti-aliasing window is a wedge with its apex at the origin. For a given value of p, we now determine the parameters of the window. For the present we assume v_{rms} is constant and of known value.

Observing Figure 3 of Slant Plane Wave Interpretation Coordinates (this report, page 184), we wish to find a relation between t and f. This has already been derived in Velocity Estimation in Slant Frames I (this report) and is its equation (5b), page .

$$t_m(f) = \frac{f}{p\,v^2} \tag{7}$$

where, for the present derivation, t_m will denote that value of time (given f, p, and v) which contains energy at the precise p value of interest. In other words, $t_m(f)$ will denote the points of tangency as seen in Figure 4.

We wish to include all energy into the summation which propagates within some range $\Delta\theta$ from the main angle of propagation, θ. We now define the quantities

$$t_{min}(f) = \frac{f}{p_{max}\,v^2} \tag{8a}$$

and

$$t_{max}(f) = \frac{f}{p_{min}\,v^2} \tag{8b}$$

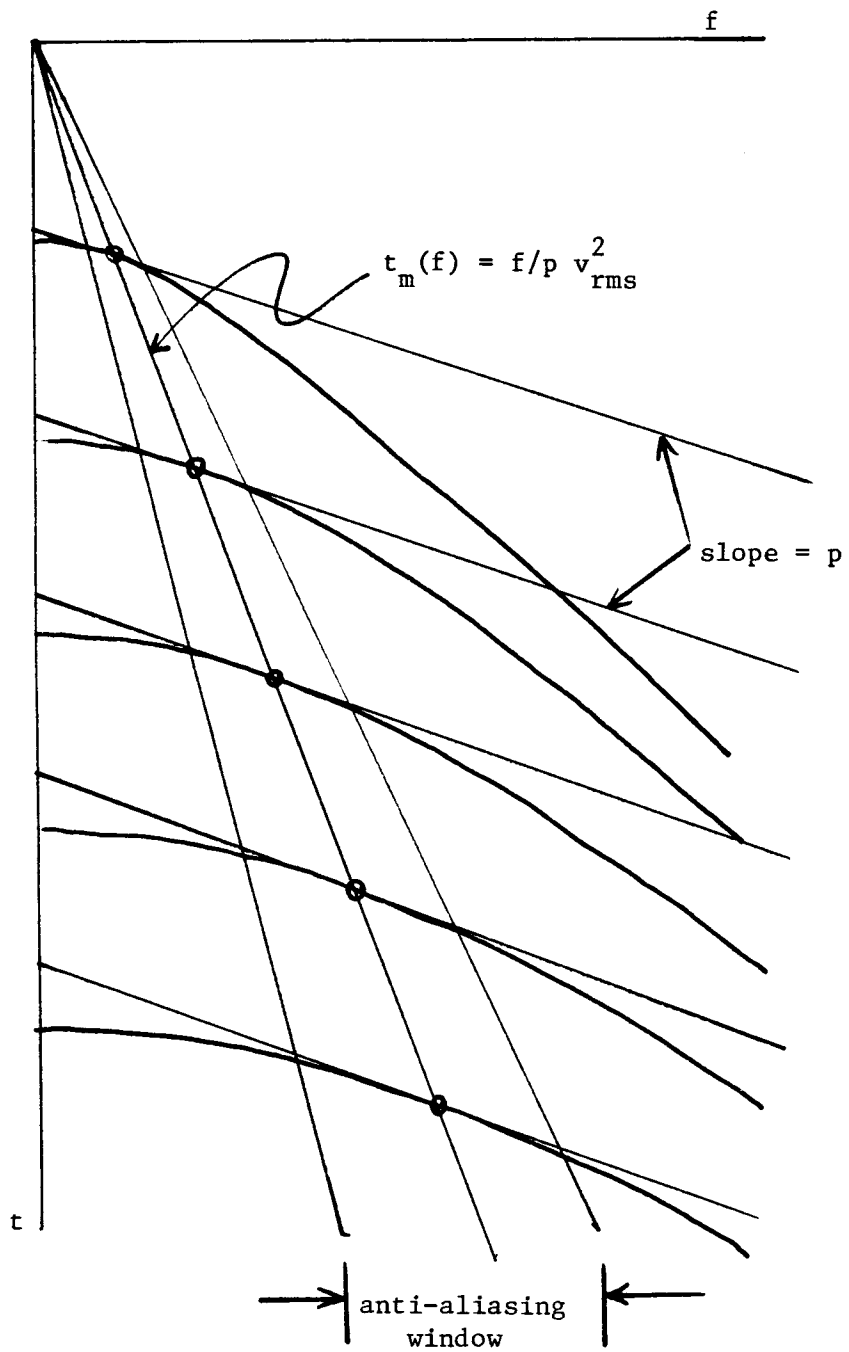

Figure 4.

The anti-aliasing window. If we include only data in the narrow range shown in the figure, the slant summation will never produce aliased energy. To have knowledge of the optimum window shape, however, requires knowledge of both rms velocity and structural dip as a function of time. The parameters of the window can be made to include more than the minimum data required, since we presumably have only estimates of velocity and structural dip.

A structural dip of $\pm\phi$ affects the anti-aliasing window by shifting the mean window position from θ_m to $\theta_m \pm 2\phi$. So, unknown dip can be compensated by making $\Delta\theta$ as large as possible.

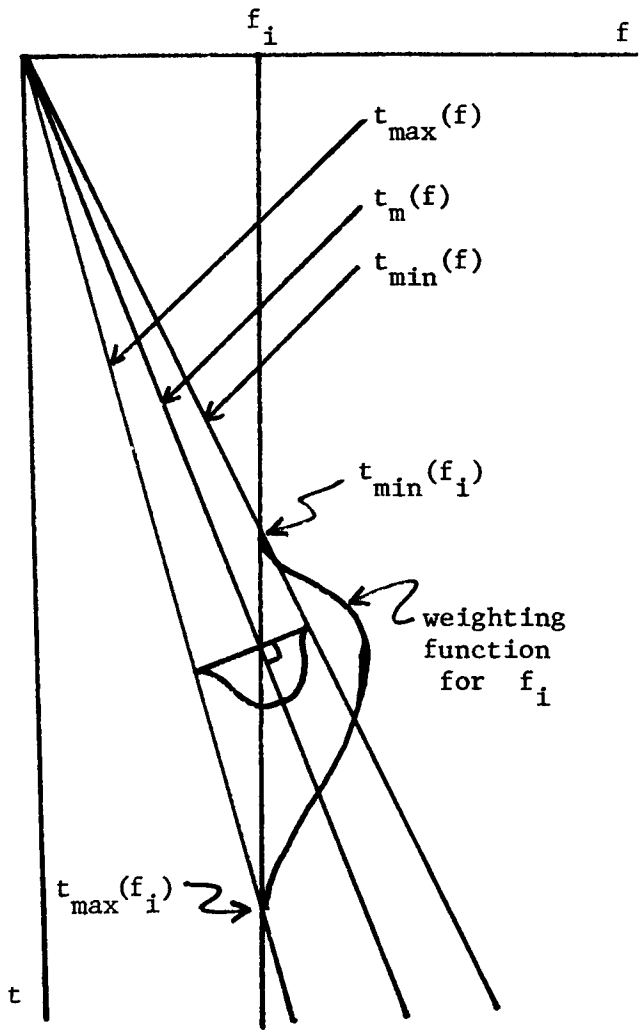

Figure 5. The anti-aliasing window of Figure 4 shown with a weighting function applied. As described in the text, we wish to design a tapering function along a perpendicular to the main radial trace. This can then be projected on to a single trace, producing a set of weights along a trace. One can show by similar triangles that for a given value of p , the weighting function for a single trace thus determined is identical to the weighting functions for all traces in the gather but with some simple scaling factors.

Now since

$$p = \frac{\sin\theta}{v} \tag{9}$$

we write

$$p_{min} = \frac{\sin(\theta-\Delta\theta)}{v} \tag{10a}$$

and

$$p_{max} = \frac{\sin(\theta+\Delta\theta)}{v} \tag{10b}$$

or

$$p_{min} = \frac{\sin[\arcsin(pv) - \Delta\theta]}{v} \tag{11a}$$

and

$$p_{max} = \frac{\sin[\arcsin(pv) + \Delta\theta]}{v} \tag{11b}$$

Combining equations (11) with (8),

$$t_{max}^{min}(f) = \frac{f/v}{\sin(\arcsin(pv) \pm \Delta\theta)} \tag{12}$$

So, equation (12) shows that the two quantities t_{max} and t_{min} are determined by the fixed quantity $\Delta\theta$. Setting the value of $\Delta\theta$ determines the size of the anti-aliasing window. Claerbout showed (SEP-5, p. 6) that if $2\Delta\theta \cong 12°$ then the window includes the first Fresnel zone. We will always want to make this quantity somewhat larger to compensate for errors in first velocity estimate, structural dip, and energy contributing to the stack from near to, but outside the first Fresnel zone. The figures at the back of this section show slant stacks at various values of $\Delta\theta$.

Equation (12) gives the window for a constant velocity medium. The generalization of (12) to $v = v(z)$ is not as simple as replacing

v with $v_{rms}(z)$, but a similar formula to (12) can be derived.

The taper on the anti-aliasing window was made to be the cosine function

$$\text{taper}(\delta\theta) = \frac{1}{2}\left[\cos\left(\frac{\pi\,\delta\theta}{\Delta\theta}\right) + 1\right] \qquad (13)$$

where $\delta\theta$ is the deviation of the propagation angle from the main angle, θ_m , which is predicted from $p = \sin\theta_m / v$.

Now, for some value of time and offset in a common shot gather,

$$\delta\theta(f,t) = \theta_m - \theta(f,t) = \sin^{-1} p\,v - \sin^{-1}\left(\frac{f}{vt}\right) \qquad (14)$$

So, equation (12) defines the limits of the anti-aliasing window, while (13) and (14) define the taper, depicted in Figure 5.

Figures (6) through (12) show slant stacks on synthetic gathers using the methods just described to reduce end effects and aliasing. Figure 6 shows the synthetic gather from which all the slant stacks were made. All figures have the same amplitude scaling (they clip at the same amplitude) and show to what extend the slant stacked data is a partial coherency stack.

The methods described here are not intended to be the last word on the subjects of end effect and aliasing reduction. They are a first-stab at these troublesome problems, and they have the advantage of being computationally cheap. (It takes less CPU time to perform a slant stack with the end effect reduction and anti-aliasing window than without them.)

Some clear deficiencies exist, however, in the realm of velocity estimation. This becomes clear from the final figures which indicate trouble when v_{stk} differs from the true velocity by more than 20%. This is hardly an adequate situation when velocity estimation is the

intent. More robust techniques must yet be developed which do a better job at estimating traces off the ends of the gather.

On the positive side, given that we know the depth-dependent velocity to within 10% and the structural dip, we can slant stack any field data without worry of end effects or aliasing.

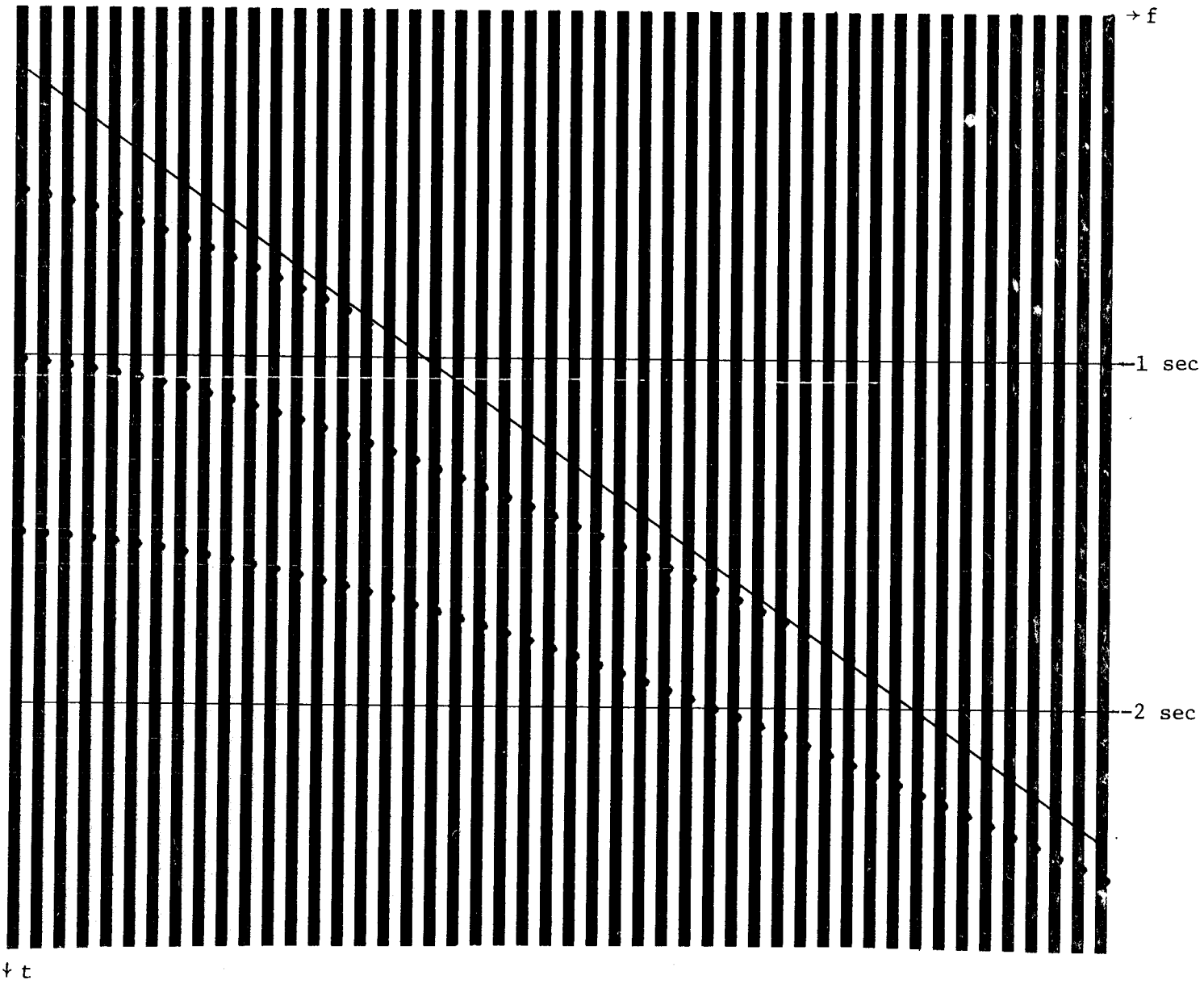

Figure 6. The common shot (or geophone) gather from which all subsequent plots of slant stacks were created. A constant velocity of 5700 fps was used, and a mute was introduced (shown as the diagonal straight line). This and all subsequent plots have the same amplitude scaling factor (all clip at the same amplitude) showing that the slant stack is a partial coherency stack. Waveform sizes should be compared with care since this figure has a different time scale than those subsequent. The stack does indeed stretch the waveform, but apparently by only 10% (more or less). For trace i, the offset is $966 + 220i$ feet.

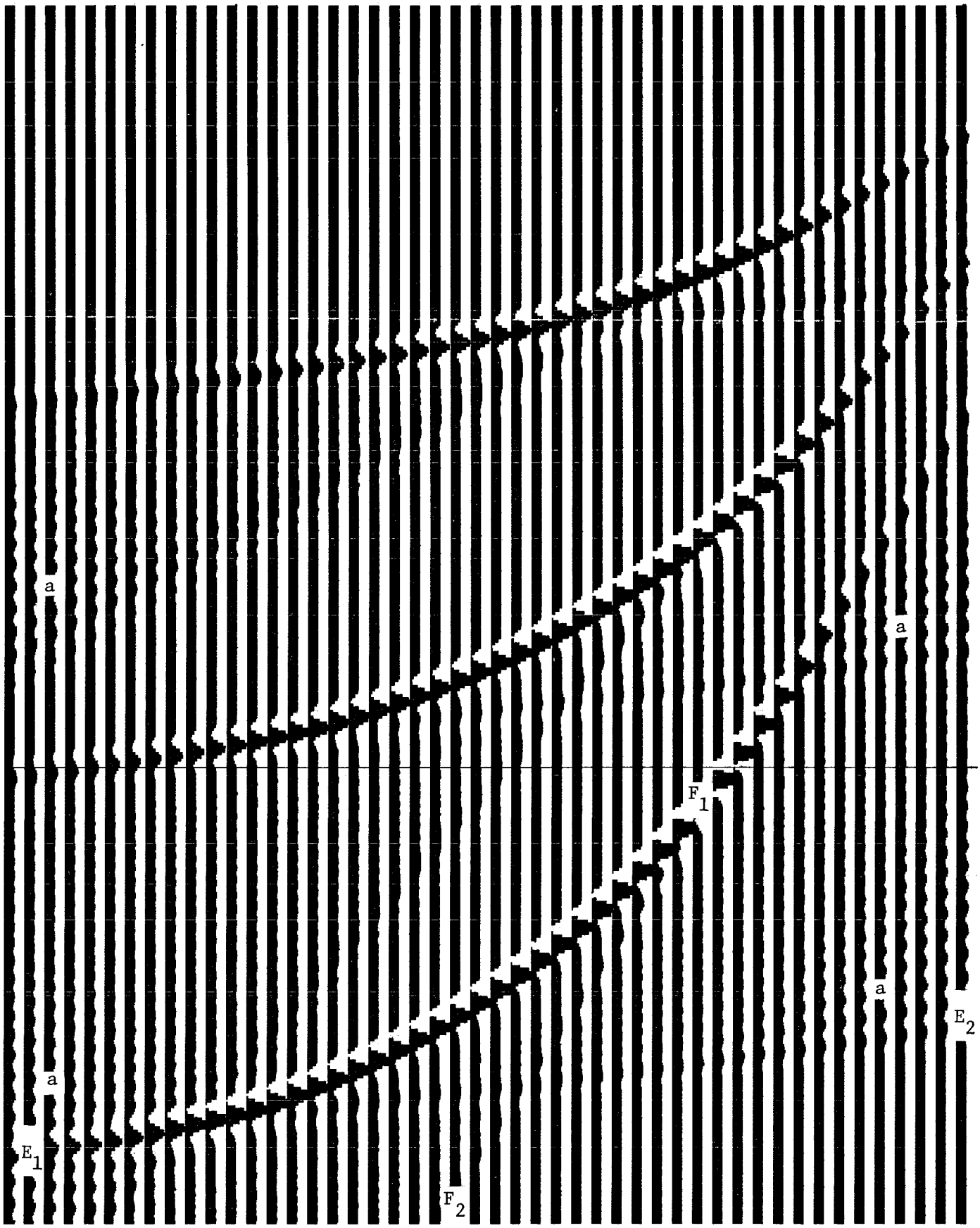

Figure 7. The data of Figure 6 slant stacked with no provision for eliminating end effects or aliasing. End effects are labeled on the third event, E_1E_2 for the near trace, and F_1F_2 for the far trace. Compare with Figure 1. Aliasing is evident in regions labeled "a".
(cont'd. on following page)

Fig. 7 (Cont'd.)

The amplitude scaling is the same as that in Figure 6; note, however, that the time scales are different. Careful measurement of waveform lengths show a very small increase from the originals in Figure 6. The stacking parameter, p, increases from left to right, and for trace i, the value of p is $i / (48 \times 5800)$. The "true" material velocity is 5700 f/s.

Figures 8 - 12

Slant stacks with end effect reduction and anti-aliasing window as described in the text. These figures all have the same amplitude scaling, as do Figures 6 and 7. The v_{stk} parameter is the input velocity used in the end effect and anti-aliasing reduction, and $\Delta\theta$ is the window width parameter. See equations (6), (12), (13), and (14) in the text. The "true" velocity for all plots is 5700 f/s.

The p and t axes are scaled the same as they are in Figure 7. Figures 11 and 12 have a lower upper limit for p because they were created with a higher value of v_{stk}, and the largest permissible value of p in the anti-aliasing window calculation is $p = 1/v_{stk}$.

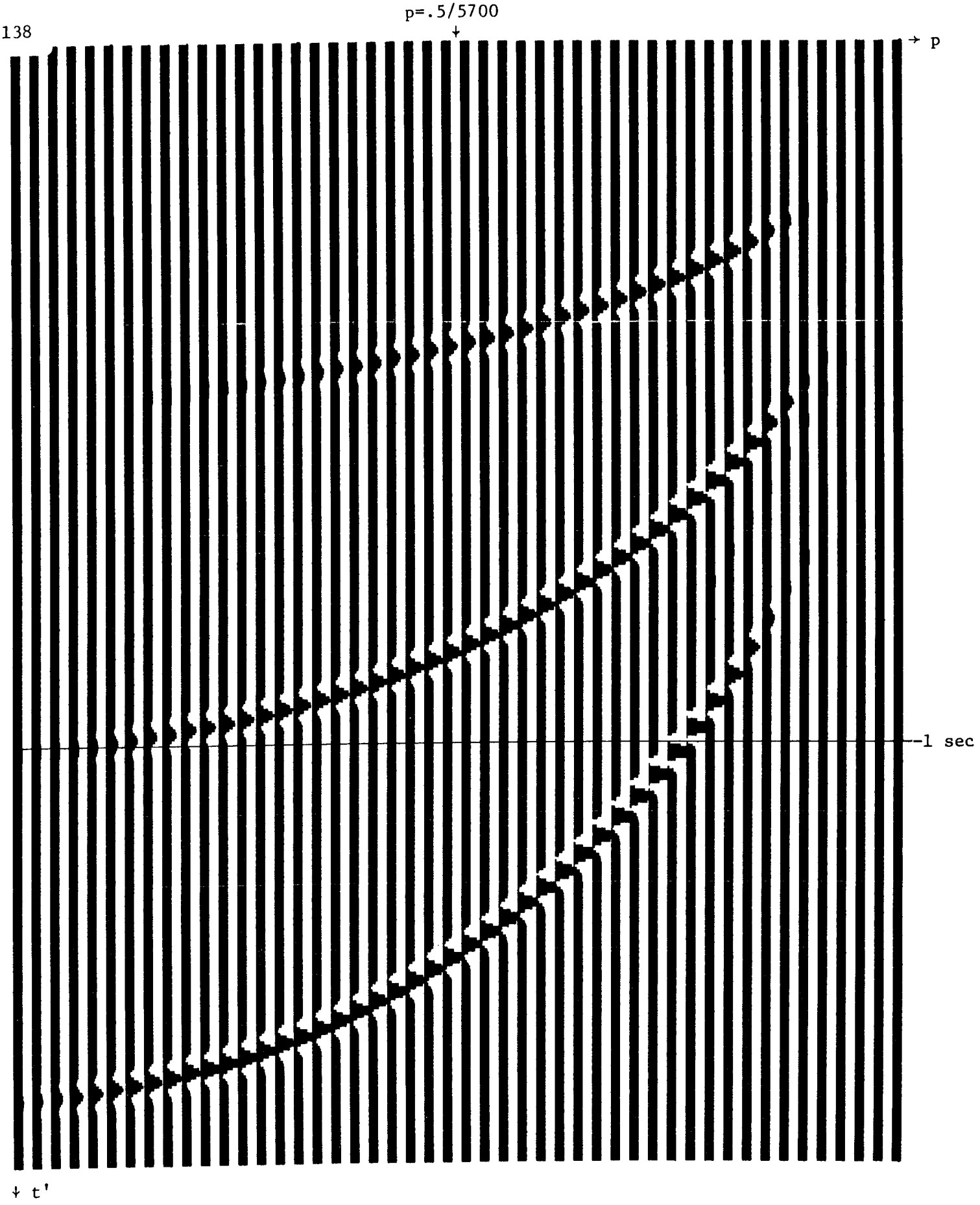

Figure 8a. $v_{stk} = 5700$, $\Delta\theta = 10°$

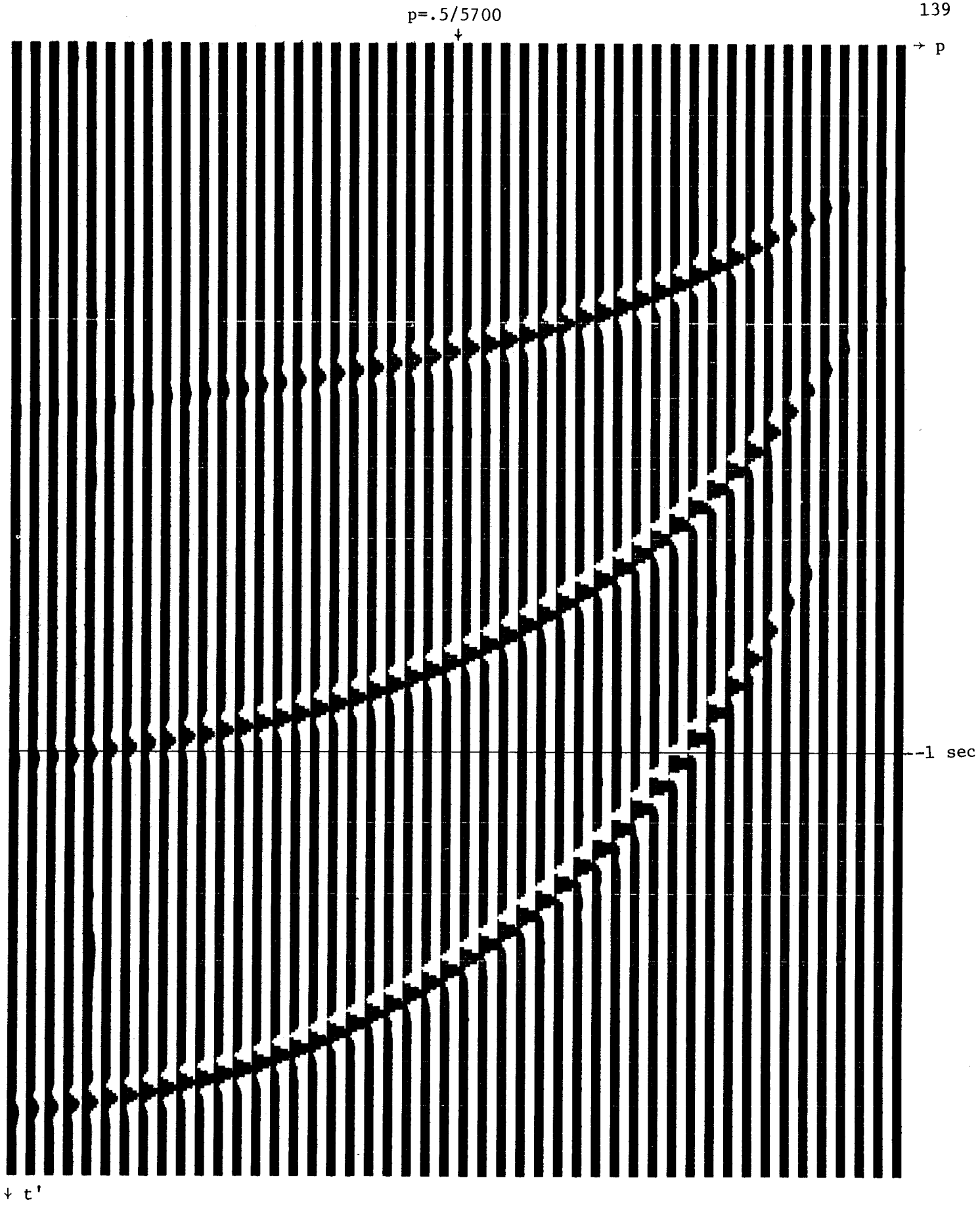

Figure 8b. v_{stk} = 5700 , $\Delta\theta$ = 20°

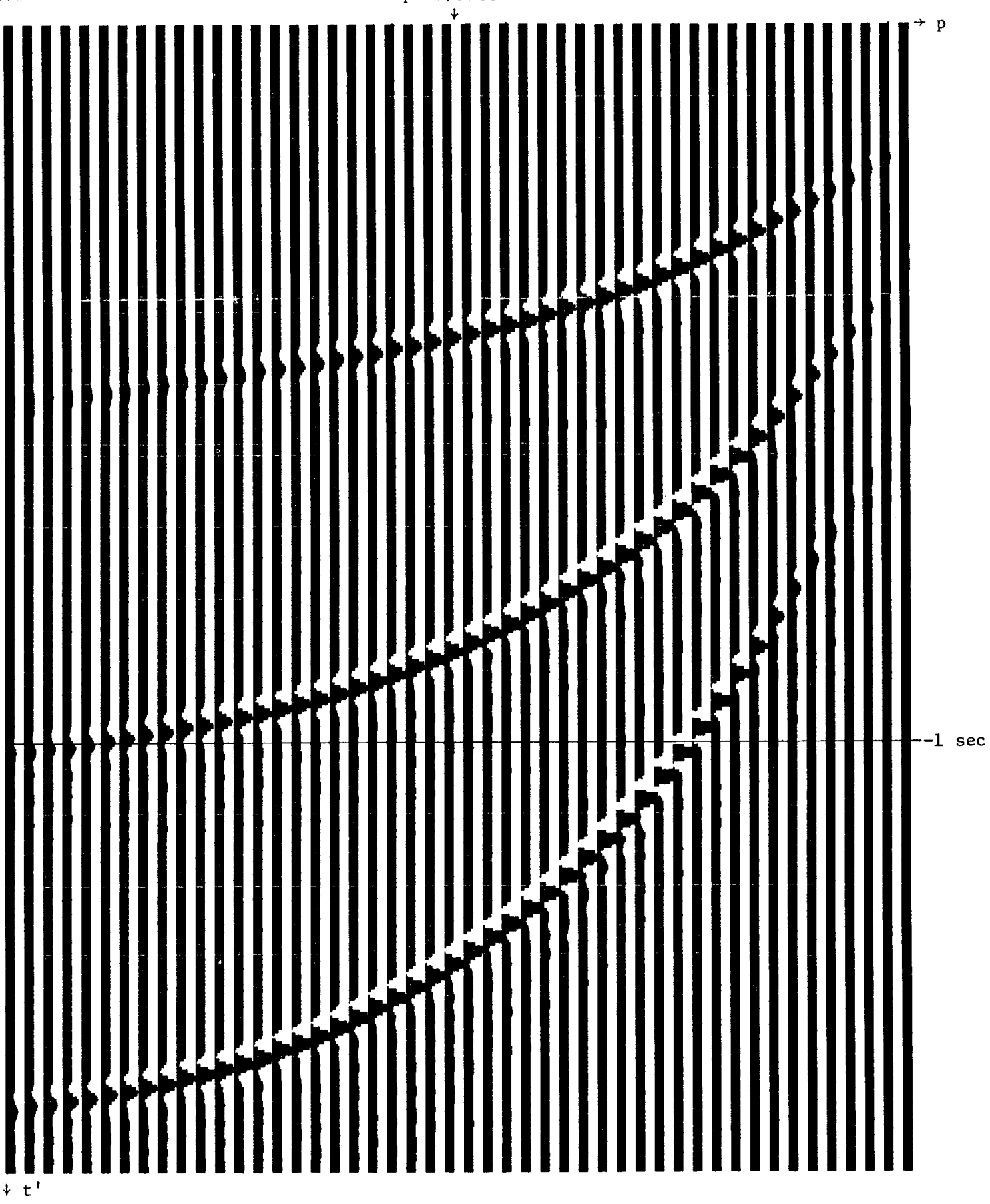

Figure 8c. v_{stk} = 5700 , $\Delta\theta$ = 30°

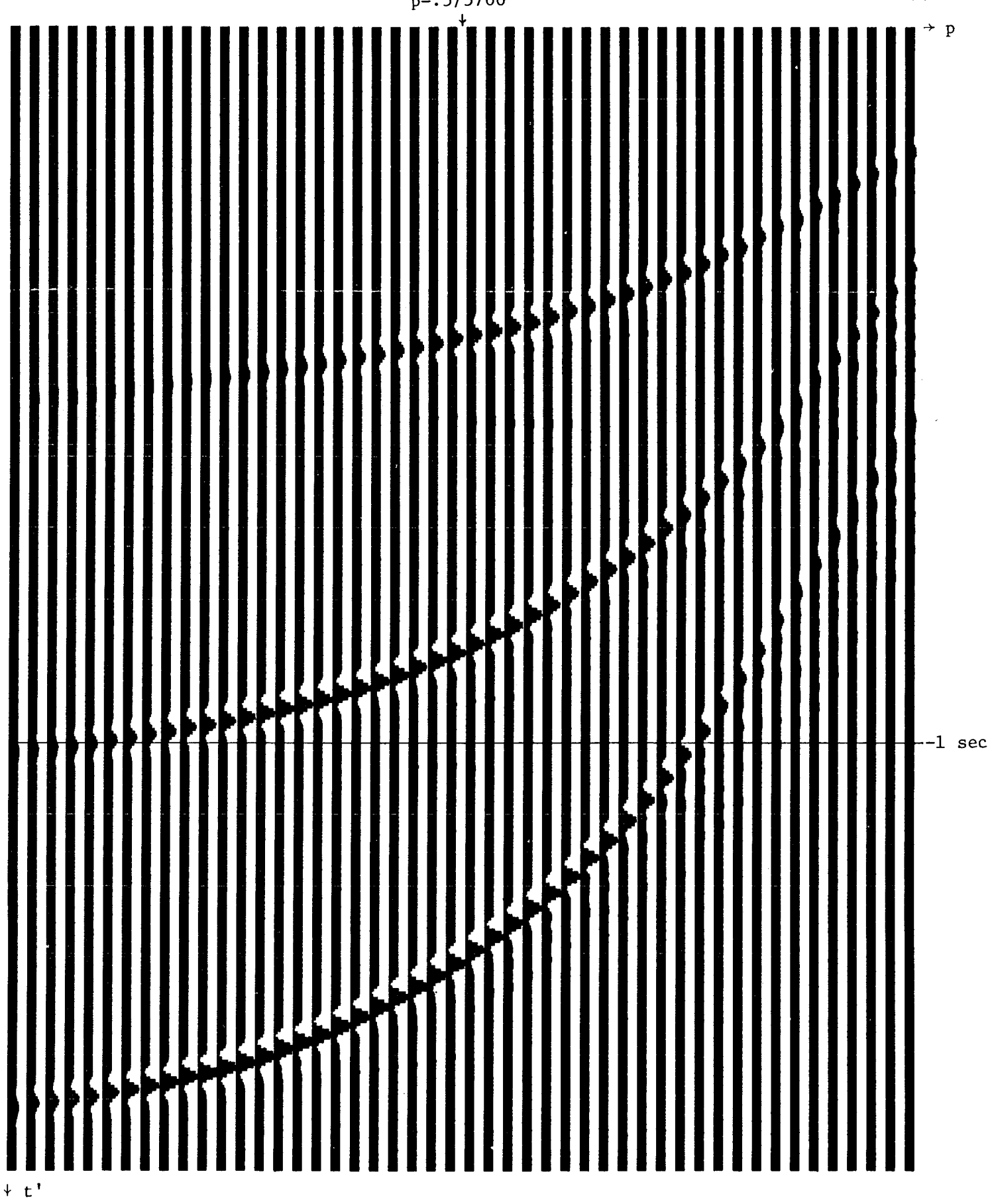

Figure 9a. v_{stk} = 90% of 5700 , $\Delta\theta$ = 20°

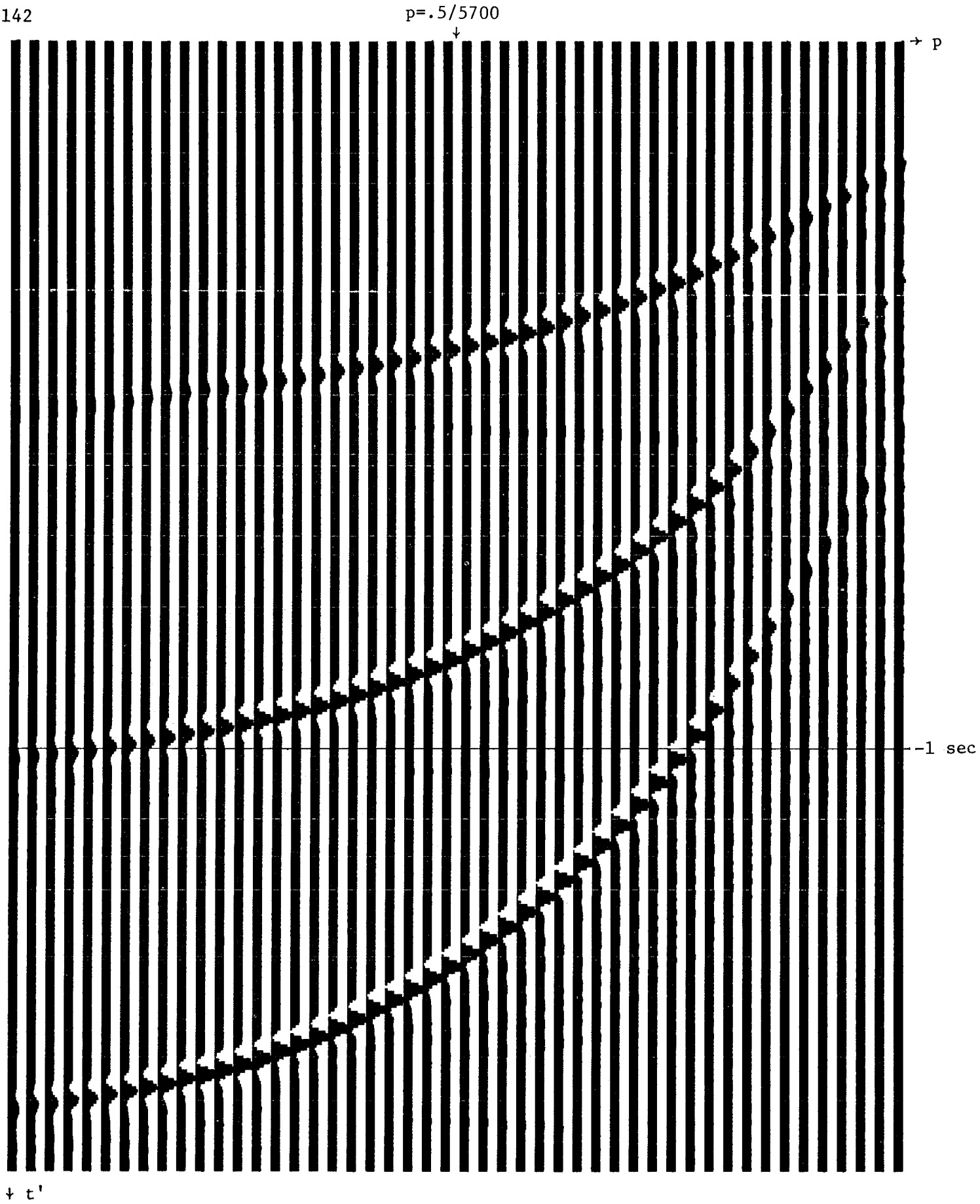

Figure 9b. v_{stk} = 90% of 5700 , $\Delta\theta$ = 30°

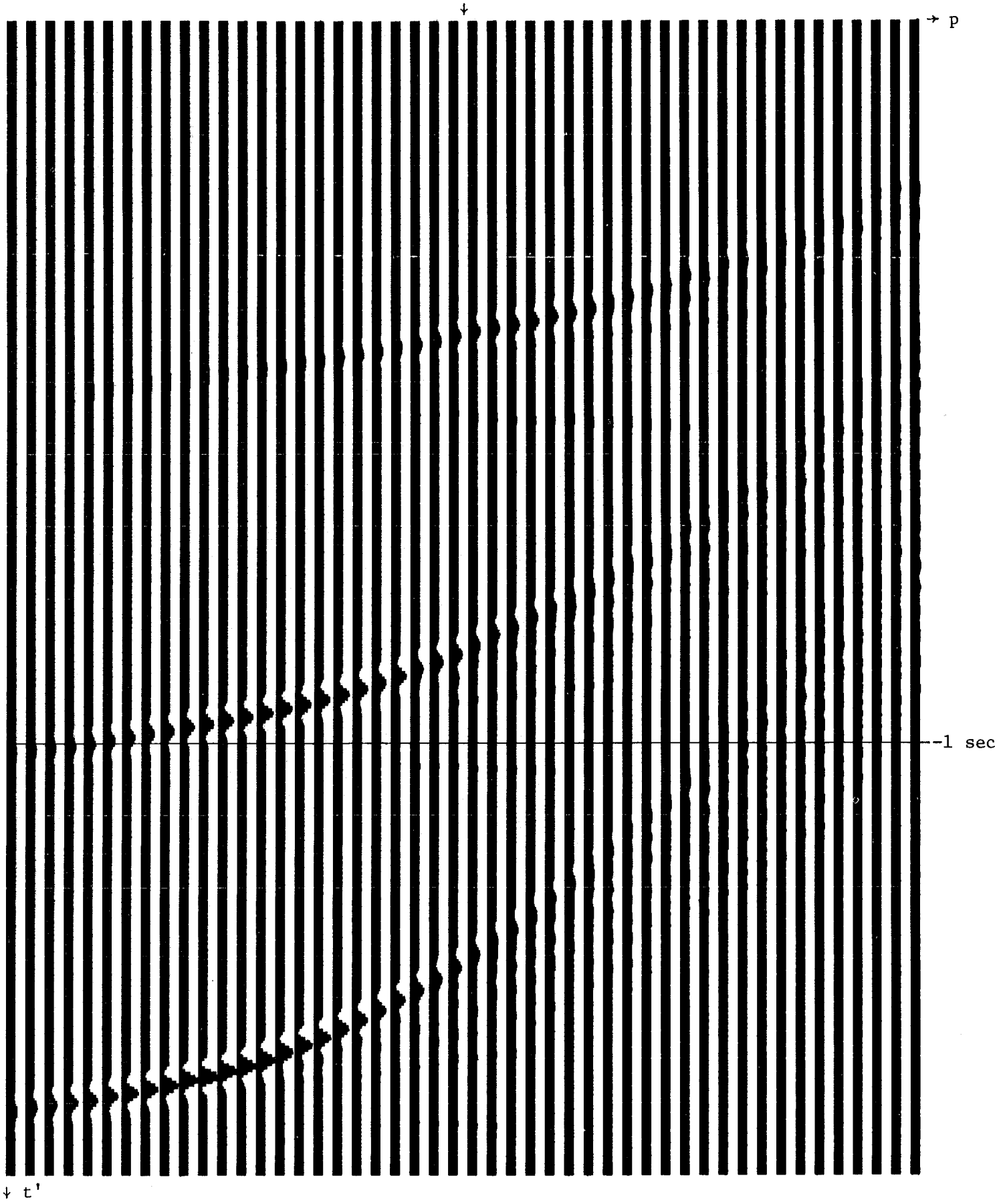

Figure 10a. v_{stk} = 80% of 5700 , $\Delta\theta$ = 20°

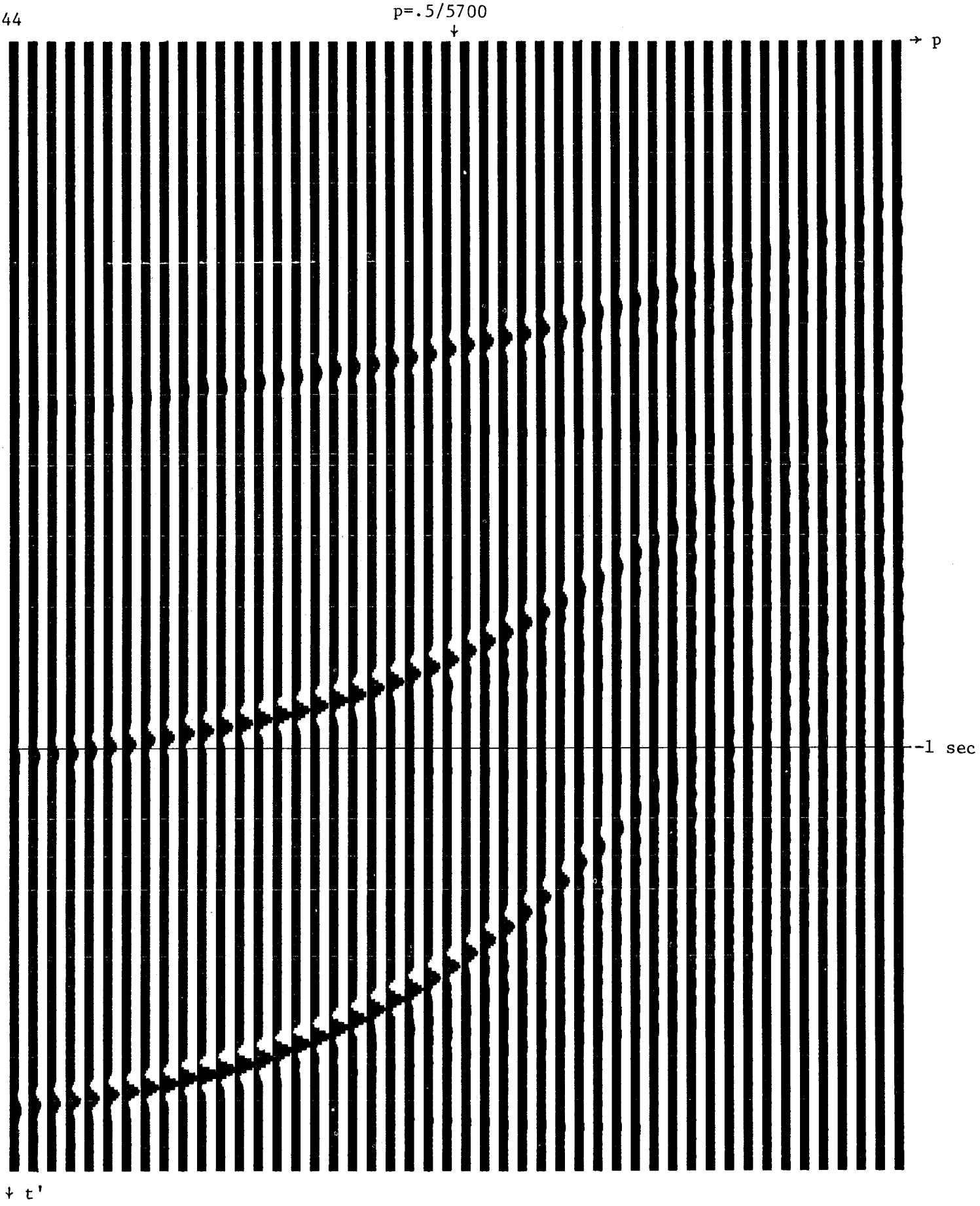

Figure 10b. v_{stk} = 80% of 5700 , $\Delta\theta$ = 30°

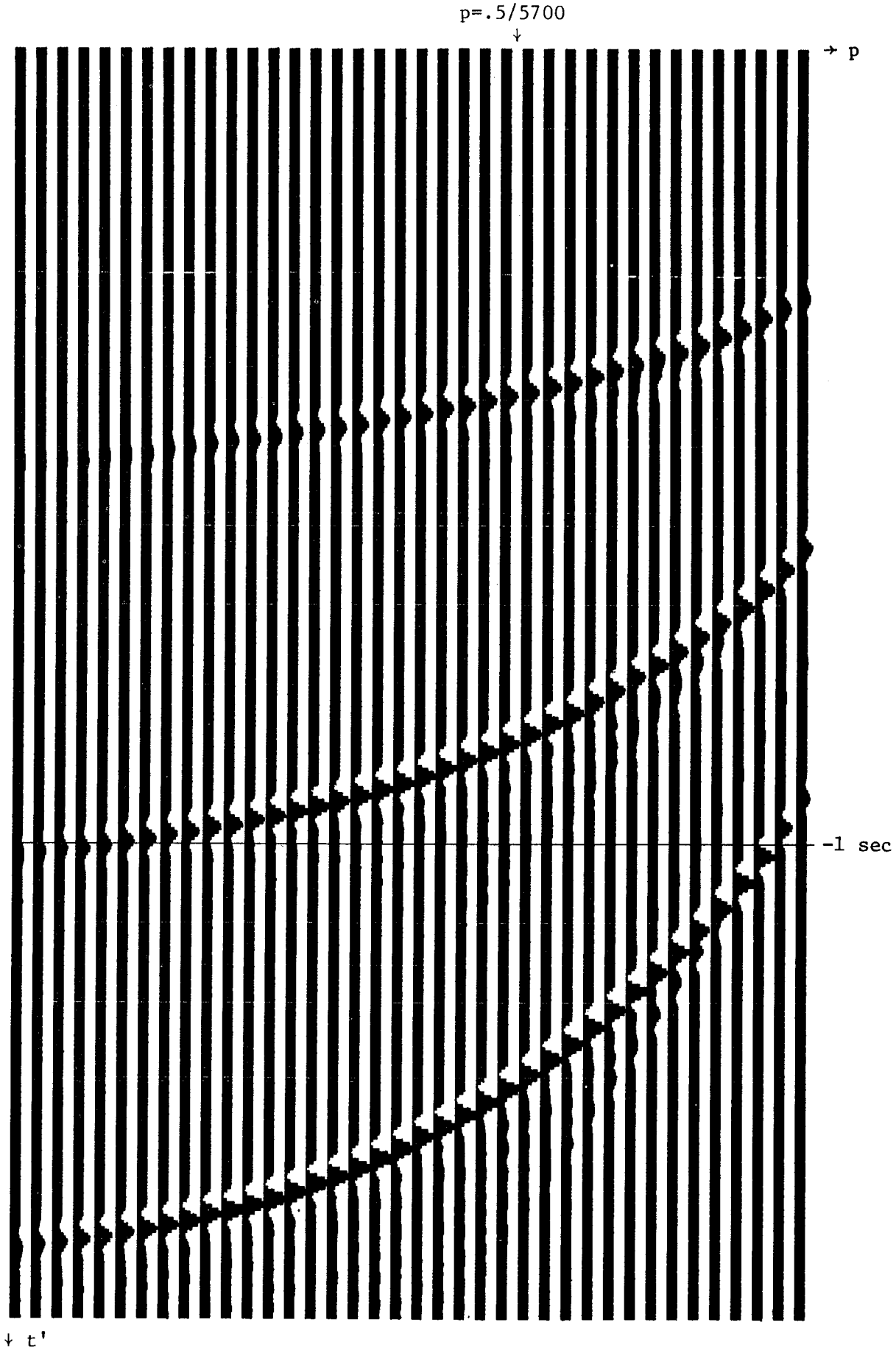

Figure 11a. v_{stk} = 110% of 5700 , $\Delta\theta$ = 20°

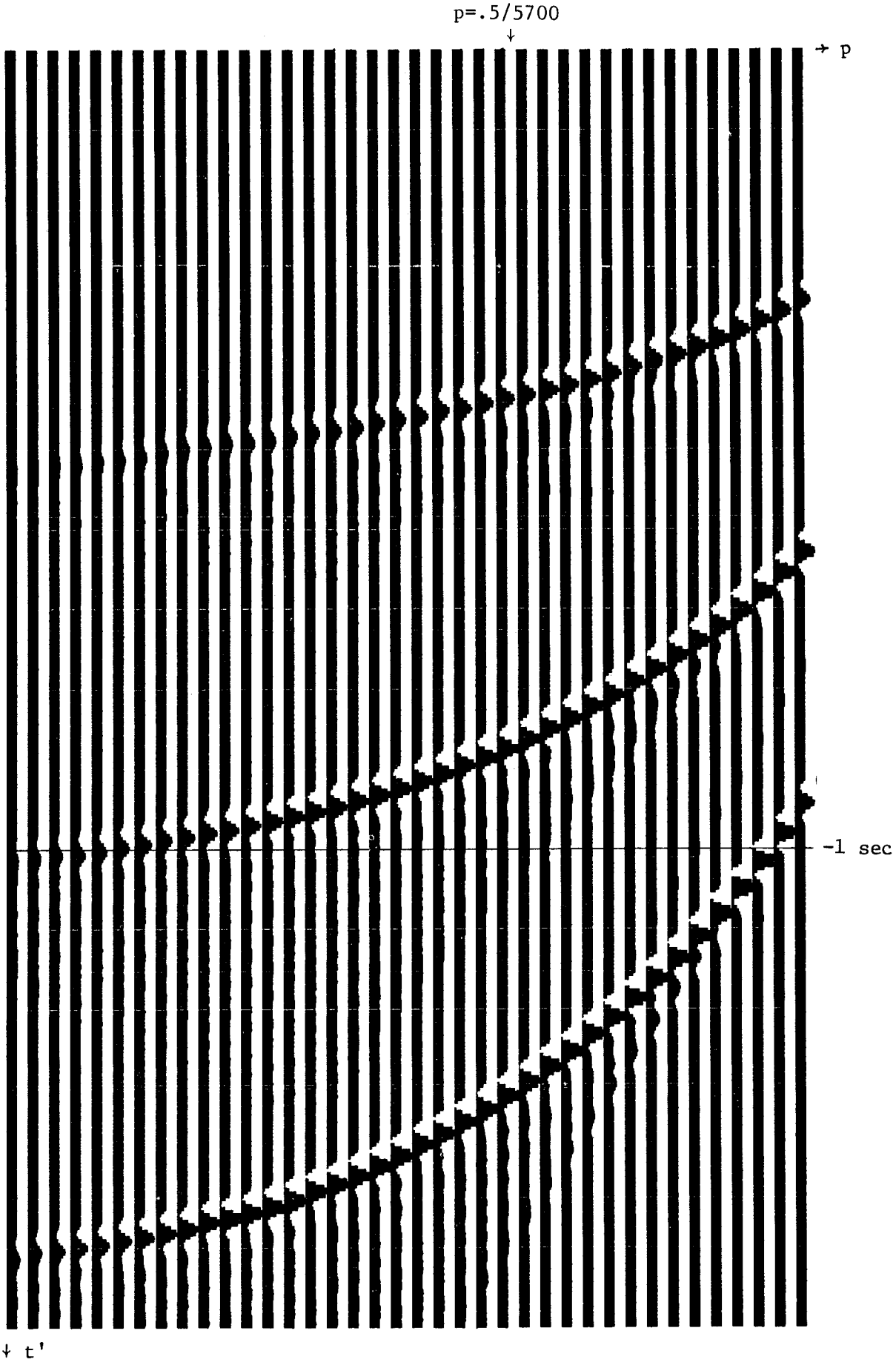

Figure 11b. v_{stk} = 110% of 5700 , $\Delta\theta$ = 30°

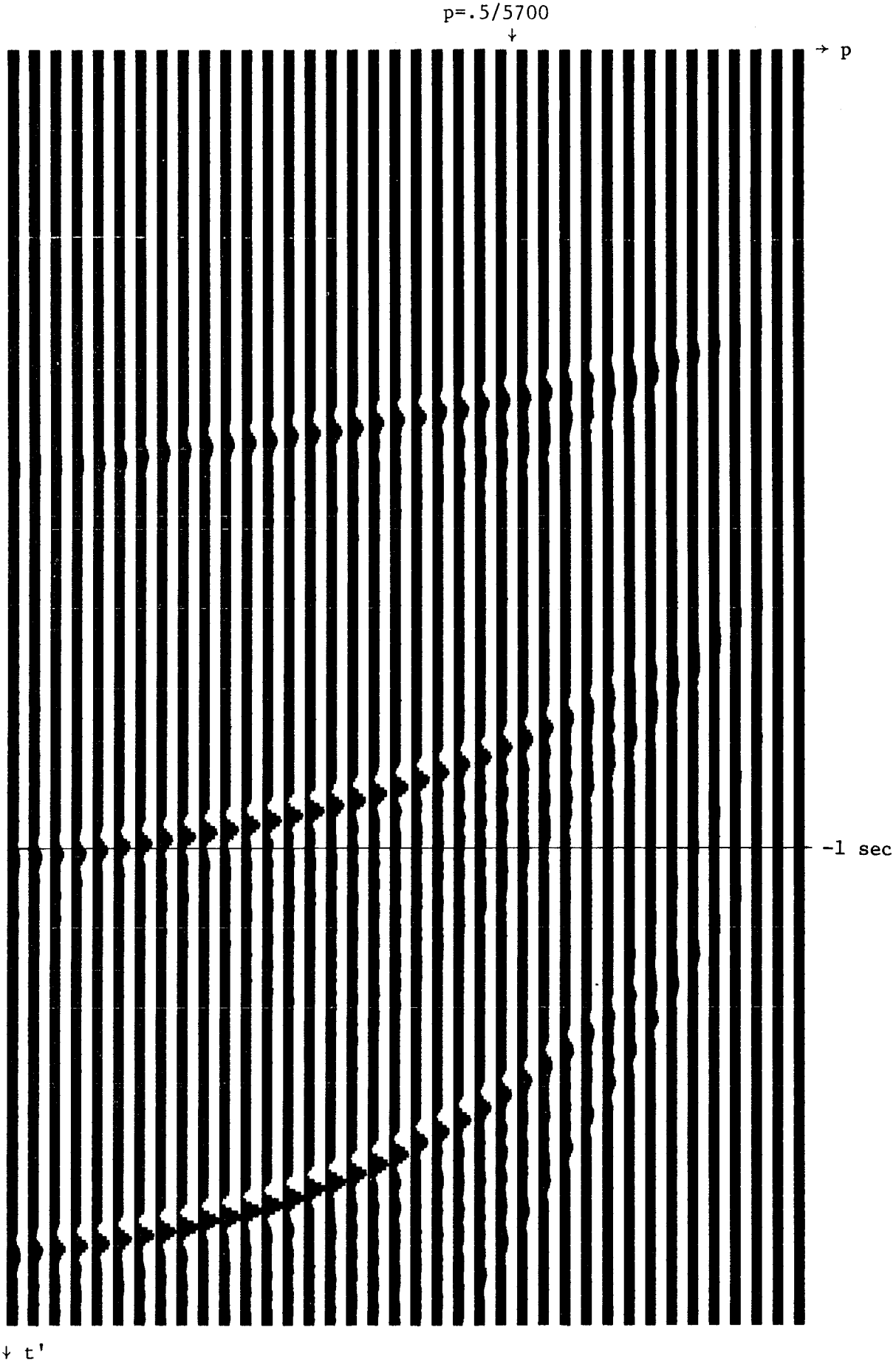

Figure 12a. v_{stk} = 120% of 5700 , $\Delta\theta$ = 20°

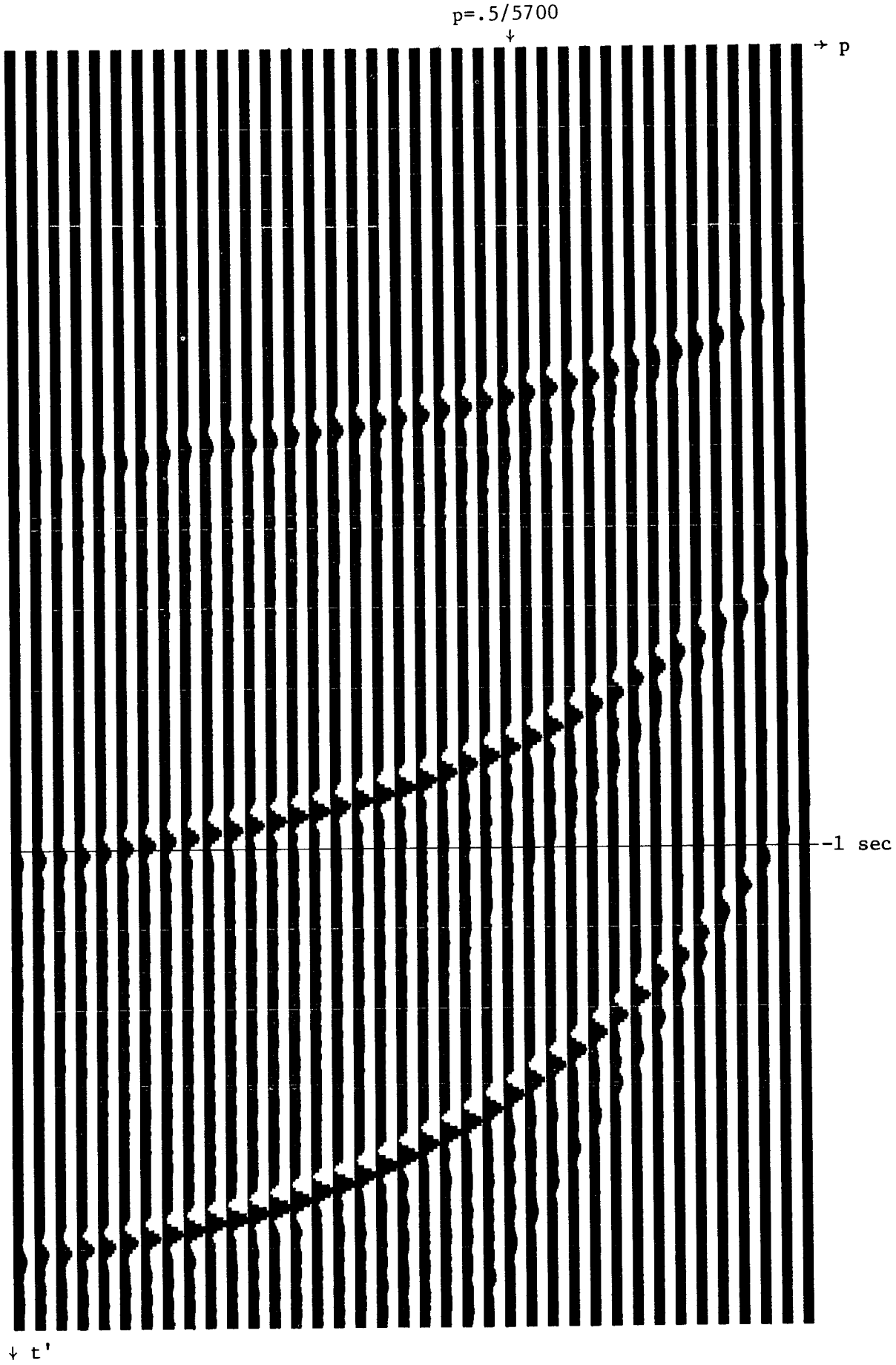

Figure 12b. v_{stk} = 120% of 5700 , $\Delta\theta$ = 30°